Marquette University
e-Publications@Marquette

Electrical and Computer Engineering Faculty Research and Publications

Electrical and Computer Engineering, Department of

3-2006

On Innovative Methods of Induction Motor Interturn and Broken-bar Fault Diagnostics

Behrooz Mirafzal
Marquette University

Nabeel Demerdash
Marquette University, nabeel.demerdash@marquette.edu

Follow this and additional works at: https://epublications.marquette.edu/electric_fac

 Part of the Computer Engineering Commons, and the Electrical and Computer Engineering Commons

Recommended Citation

Mirafzal, Behrooz and Demerdash, Nabeel, "On Innovative Methods of Induction Motor Interturn and Broken-bar Fault Diagnostics" (2006). *Electrical and Computer Engineering Faculty Research and Publications*. 195.
https://epublications.marquette.edu/electric_fac/195

Marquette University

e-Publications@Marquette

Department of Electrical and Computer Engineering Faculty Research and Publications/College of Engineering

***This paper is NOT THE PUBLISHED VERSION*.**
Access the published version at the link in the citation below.

IEEE Transactions on Industry Applications, Vol. 42, No. 2 (2006, March/April): 405-414. DOI. This article is © Institute of Electrical and Electronic Engineers (IEEE) and permission has been granted for this version to appear in e-Publications@Marquette. Institute of Electrical and Electronic Engineers (IEEE) does not grant permission for this article to be further copied/distributed or hosted elsewhere without the express permission from Institute of Electrical and Electronic Engineers (IEEE).

On Innovative Methods of Induction Motor Interturn and Broken-Bar Fault Diagnostics

B. Mirafzal
Rockwell Automation Allen-Bradley, Mequon, WI
N.A.O. Demerdash
Department of Electrical and Computer Engineering, Marquette University, Milwaukee, WI

Abstract:

A fault indicator, the so-called swing angle, for broken-bar and interturn faults is investigated in this paper. This fault indicator is based on the rotating magnetic-field pendulous-oscillation concept in faulty squirrel-cage induction motors. Using the "swing-angle indicator," it will be demonstrated here that an interturn fault can be detected even in the presence of machine manufacturing imperfections. Meanwhile, a broken-bar fault can be detected under both direct-line and PWM excitations, even under the more difficult condition of partial-load levels. These two conditions of partial load and motor

manufacturing imperfections, which are considered as difficult situations for fault detection, are investigated through experimentally obtained test results for a set of 2- and 5-hp induction motors.

SECTION I. Introduction

Studies on electric-machine fault diagnostics and protection date back to the time when the manufacturers and users of electric machines initially relied on simple protections such as overcurrent and overvoltage devices to ensure safe and reliable operation. Improving power-electronic devices with the ability of switching high-rated currents at high switching frequencies led to the widespread use of motors in adjustable speed drives. Now, electric machines in conjunction with modern power-electronic devices play very important roles in many industrial plants. Knowing when an electric machine requires maintenance allows users to perform the required maintenance at their convenience rather than during costly unscheduled shutdowns. This requirement led to the study and development of concepts of modern fault diagnostics and condition monitoring of electric machines in adjustable-speed-drive systems.

In the past two decades, there have been many investigations on fault diagnostics in electric machines. Modern investigations on induction-motor fault diagnostics were started in the early 1980s—by Deleroi in 1982 [1], [2] as well as Williamson and Smith in 1982 [3]. These investigations were focused on rotor-fault analysis and detection. In 1984, Williamson and Mirzoian reported their study on stator-winding faults in induction motors [4], [5]. These investigations on induction-motor internal-fault analysis have been followed by many studies such as the work of Kliman et al. [6], [7], Bellini et al. [8], Trutt et al. [9], Kral et al. [10], Schoen et al. [11], Lee et al. [12], Vas [13], Benbouzid and Kliman [14], Kostic-Perovic et al. [15], Arkan et al. [16], Demian et al. [17], Henao et al. [18], Cruz and Cardoso [19], and Nandi and Toliyat [20]. This is in addition to others who have performed various investigations in electric machines and drives fault diagnostics [21]–[22][23][24][25]. In the modeling of internal faults in electric machines, which enables one to study the effect of faults on motor performance, two approaches mainly stand out—the winding-function-based approach [26] and the time-stepping finite-element-based approach [27].

In general, squirrel-cage induction-motor faults can be categorized into electrical and mechanical faults. Electrical faults/asymmetries can be also categorized into rotor and stator faults. All these possible faults in induction motors and their associated subsets are summarized as depicted in the block-diagram schematic of Fig 1.

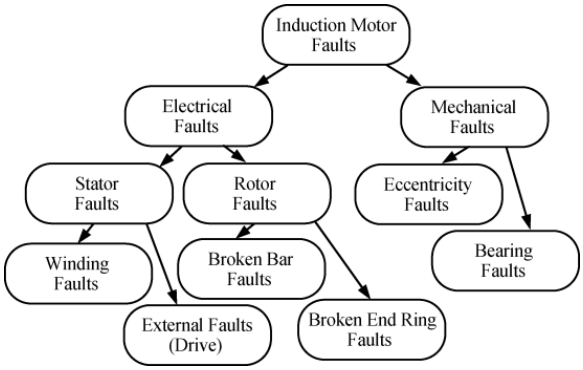

Fig 1. Block diagram of induction-motor fault categories.

The statistical report of the Motor Reliability Working Group of the IEEE-Industry Applications Society (IAS), which surveyed 1141 motors, [28], [29] and the Electrical Power Research Institute (EPRI), which surveyed 6312 motors, [30] are summarized here in TABLE I. As one can observe, bearing-(mechanical) and winding (stator)-related failures are the dominant trouble areas. Moreover, the percentage of winding- and rotor-related failures is around 40%, and thus form an important area of research. Hence, the authors find it pertinent to deal with these two electrical types of component failure.

TABLE I Percentage of Failures by Major Motor Component

Major Components	IEEE-IAS [28], [29] % of Failures	IPRI [30] % of Failures
Bearing Related	44	41
Winding Related	26	36
Rotor Related	8	9
Other	22	14

Accordingly, while discussing these two electrical types of motor component failure, this paper addresses two major problems:

1. detection of broken-bar fault, when a motor is energized by direct line and when energized by a pulsewidth-modulation (PMW)-based drive, under different load levels;
2. detection of incipient interturn fault in the presence of a degree of motor manufacturing imperfection and under different load levels.

The basis of the present techniques for detecting a broken-bar fault and an interturn fault is to monitor the orientation of the axis of the induction machine's resultant magnetic field, and hence compute (estimate) the range of its oscillation due to the aforementioned types of faults in a synchronously rotating frame of reference. The range of this oscillation is referred to here as the “swing-angle” index. Meanwhile, the swing angle is measured differently for detecting a broken bar and an interturn fault. Thus, they are identified differently, namely, $\Delta\delta_1$ and $\Delta\delta_{\mathrm{sc}}$, for rotor broken-bar and stator interturn short-circuit faults, respectively.

SECTION II. Swing-Angle Calculation Using Motor Terminal Space-Vector Quantities

It has been shown in earlier papers that the range of the pendulous oscillation of a motor's magnetic-field space vector progressively increases with an increase in the number of broken bars [24], [25]. It will be shown here that this pendulous oscillation also progressively increases in cases involving a correspondingly increasing number of interturn stator-winding shorts, specifically as the loop-current magnitude in these shorted turns (STs) increases. However, the two pendulous oscillations caused by interturn and broken-bar faults are different in their nature [31]. The difference between the two types of pendulous-oscillation plots will be explained later on in this paper in terms of the frequencies of the components of the indexes and their corresponding polar plots. In Fig 2, the differences between the processes that lead to the calculation of the swing angles for broken-bar and interturn faults are shown. This difference in the nature of the pendulous oscillations caused by broken-bar and interturn

faults requires different data-processing approaches for calculating the swing angle. The process of calculating swing angles for the broken-bar fault can best be summarized by the following steps.

1. The motor terminal currents and voltages are measured through current and voltage sensors and consequently digitized using an analog-to-digital (A/D) converter.
2. The output signals of the A/D converter are filtered using a low-pass filter (LPF) for the process of calculating the broken-bar swing angle (the filtering can be performed offline after the next step; see also Fig 3).
3. The output signals of the LPF are collected throughout a period of time greater than a slip cycle, because the resulting periodic phenomenon repeats itself once every half slip cycle.
4. The output signals of the previous step are used to calculate the space vectors of the voltages $\vec{v}_s$ and currents $\vec{i}_s$ throughout the aforementioned period, and consequently, the pendulous-oscillation angle $\delta(t)$ and the radius $r(t)$, which are defined as follows

$$\delta(t) = \angle\vec{i}_s(t) - \angle\vec{v}_s(t), \text{ where} 0 < \delta(t) < 2\pi \text{rad}$$

$$r(t) = \text{abs}\left(\text{Re}\left(\vec{i}_s(t)\right)\right), \text{ where} r(t) > 0.$$

(1) (2)

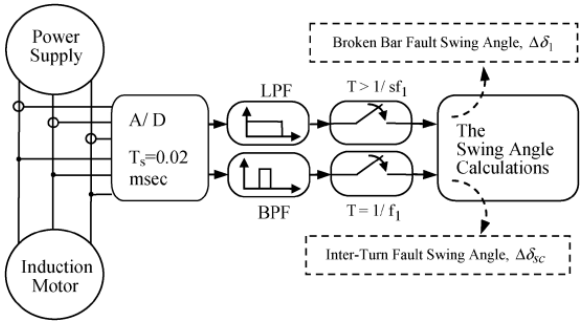

Fig 2. Functional block diagram of the swing-angle calculation for broken-bar faults and interturn faults.

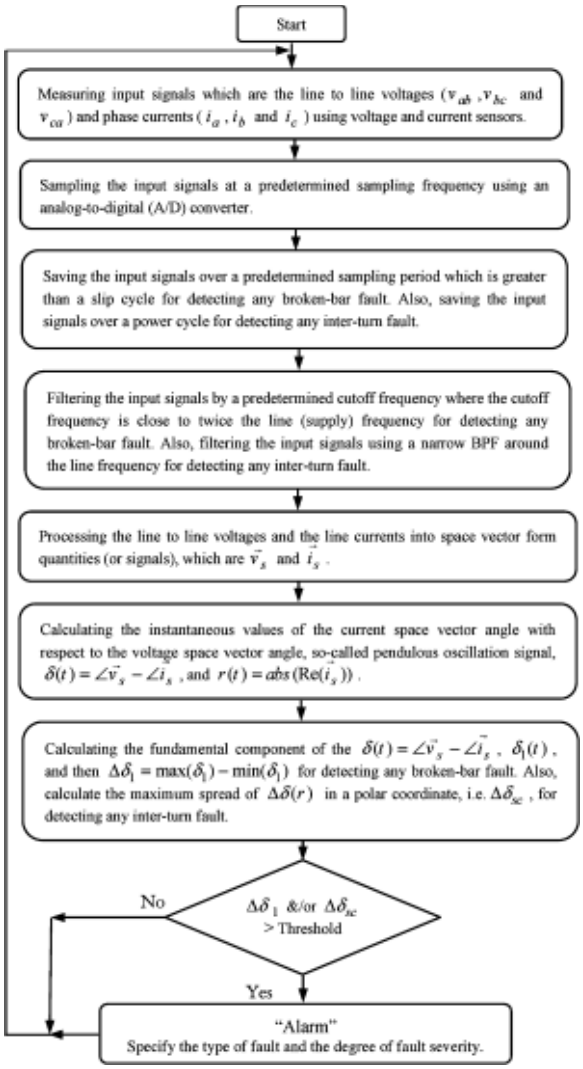

Fig 3. Flowchart diagram of the swing-angle fault-diagnosis indexes.

Remark 1

In (2), the absolute value of the real part of the space vector of the currents is used. This provides more information in the polar plot of (r, δ) for the purpose of fault identification/classification, which will be seen later on in Section III.

Here, $\vec{i}_s(t)$ and $\vec{v}_s(t)$ are defined as follows:

$$\vec{i}_s(t) = \frac{2}{3}((i_a - i_b) + \alpha(i_b - i_c) + \alpha^2(i_c - i_a))$$

$$\vec{v}_s(t) = \frac{2}{3}(v_{ab} + \alpha v_{bc} + \alpha^2 v_{ca})$$

(3) (4)

where $\alpha = \exp(j2\pi/3)$ is a space-vector operator and v_{ab}, v_{bc}, and v_{ca} are stator terminal line-to-line voltages and i_a, i_b, and i_c are stator terminal line currents.

Remark 2

In (3), these sets of current differences, $i_a - i_b$, $i_b - i_c$, and $i_c - i_a$, are used instead of the phase currents. This has two benefits. First, it should be noted that space-vector quantities are defined for a set of quantities, the summation of which is always equal to zero. Second, the outputs of current sensors typically contain undesired dc offsets; these undesired dc offsets are eliminated using the aforementioned sets of current differences.

In the case of broken-bar fault diagnosis, in order to distinguish a cage with a bar breakage from a healthy cage, even in the presence of inherent measurement and system noises, the peak-to-peak value of the fundamental component of the waveform of the pendulous oscillation, the so-called swing angle $\Delta\delta_1$ in Fig 2, is the signal being utilized here for bar defect/breakage indication as a detection index [25].

Meanwhile, the process for calculating the swing angle for interturn faults can best be summarized by the following steps.

1. The motor terminal currents and voltages are measured through current and voltage sensors and consequently digitized using an A/D converter.
2. The output signals of the A/D converter are filtered using a bandpass filter (BPF) for the process of calculating the interturn swing angle $\Delta\delta_{\mathrm{sc}}$ (the filtering can be performed offline after the next step; see also Fig 3).
3. The output signals of the LPF are collected throughout a period equal to the period of the power-supply frequency, because the resulting periodic phenomenon repeats itself every half an ac power cycle.
4. The output signals of the previous step are used to calculate the space vectors of the voltages $\vec{v}_{\mathrm{s}}$ and currents $\vec{i}_{\mathrm{s}}$ throughout the aforementioned period, and consequently, the pendulous oscillation $\delta(t)$ and the radius $r(t)$, using (1)–(4).
5. Then, the swing angle $\Delta\delta_{\mathrm{sc}}$ is obtained by calculating the maximum spread of $\Delta\delta(r) = \delta^{max} - \delta^{min}$ in a polar-plot coordinate, as will be demonstrated in the next section of this paper. Thus, for each power cycle, a single value for the swing angle $\Delta\delta_{\mathrm{sc}}$ is obtained as a detection index.

Both detection indexes $\Delta\delta_1$ and $\Delta\delta_{\mathrm{sc}}$ are indicative of the resulting pendulous oscillation in the synchronously rotating magnetic field, which is a form of perturbation superimposed on top of the normal synchronous rotation of the field in a motor.

The two procedures summarized above for obtaining the broken-bar identification signal $\Delta\delta_1$ and the interturn short-circuit identification signal $\Delta\delta_{\mathrm{sc}}$ are depicted in the algorithmic flowchart diagram of Fig 3.

SECTION III. Experimental Results

A 5-hp six-pole 460-V set and a 2-hp two-pole 460-V set of induction motors were tested under broken-bar and interturn short-circuit faults (for further details on the particulars of the two types of motors, see the Appendix). The 5-hp motors were tested under healthy as well as one through four broken-bar faults in the presence of sinusoidal and constant volts-per-hertz PWM-based drive excitations. One of the 5-hp motors was also tested under 2, 4, 6, 8, 10, and 12 interturn short-circuit faults. The 2-hp motors were tested under healthy as well as one, three, and five broken-bar faults under different load levels and only sinusoidal excitation. One of the 2-hp motors was also tested under one through five interturn short-circuit faults. For both the 5- and 2-hp motors, the interturn short circuits were achieved through an external resistor r_{f}, a $1-\Omega$ resistor for the 5-hp motor, and a $0.8-\Omega$ resistor for the 2-hp motor, in order to emulate an incipient fault with low level of circulating current in the shorted portion of the winding. This is an evaluation of the early stages of deterioration of the quality of dielectric insulation between turns. In these tests, the data-acquisition laboratory test equipment was a National Instrument LabView SCXI-1000 device, while the sampling rate was set to be 50 000 samples per second.

A. Broken-Bar Fault Diagnostics

For a PWM-based excitation, the polar plot (r,δ) of the magnetic-field space vector, $\vec{r}=r(t)\angle\delta(t)$, and its corresponding swing angle $\Delta\delta$ obtained from laboratory testing of the 5-hp motor in case of one broken bar are shown in Fig 4. It can be observed that the polar plot of (r,δ) has a (filled) petal shape due to the fact that for any angle δ, the r value is perpetually changing from zero to its maximum value. Notice that $r=\mathrm{abs}(\mathrm{Re}(\vec{i}_{\mathrm{s}}))$. This is because of the fact that the frequency of the pendulous oscillation of δ due to a broken bar, which is $2sf_1$, is much smaller than the frequency of amplitude modulation of r, which is equal to twice the line frequency—that is, $2f_1$. The pendulous oscillation $\delta(t)$ and its fundamental component $\delta_1(t)$ versus time as well as the swing angle $\Delta\delta_1$ in degrees for healthy, one, two, and three adjacent broken-bar cases are shown in Figs. 5 –8, under a PWM excitation and full-load condition. As one can see from Figs. 5 –8, there is a definite correlation between $\Delta\delta_1$ and number of rotor broken bars and it does not lead to any uncertainty in detecting and characterizing broken-bar faults in the presence of a PWM-based excitation. Hence, to these authors, it appears that the swing angle $\Delta\delta_1$ is the index of choice for detecting a broken-bar fault.

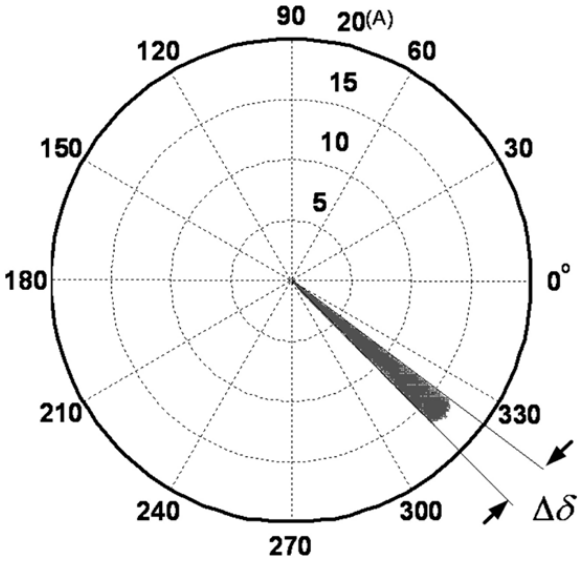

Fig 4. Polar plot (r, δ) of the magnetic-field space vector, $\vec{r} = r(t)\angle\delta(t)$, and its corresponding swing angle $\Delta\delta$ (in degrees) in the case with conditions of: one broken bar, 5 hp, PWM, and full load.

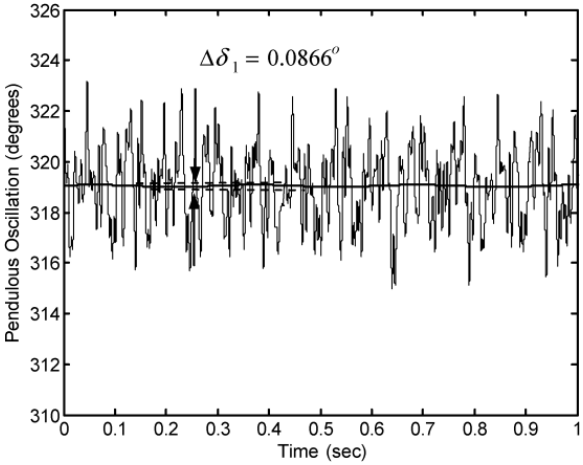

Fig 5. Pendulous oscillation and its fundamental component δ_1 (in degrees) versus time for the 5-hp motor in a healthy-situation PWM excitation.

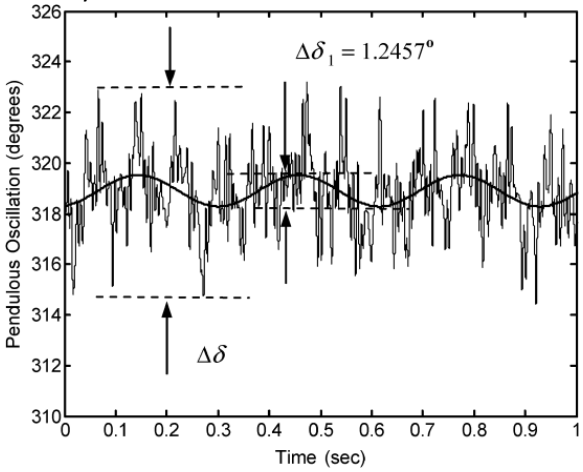

Fig 6. Pendulous oscillation and its fundamental component δ_1 (in degrees) versus time for the 5-hp motor for PWM excitation with one broken bar.

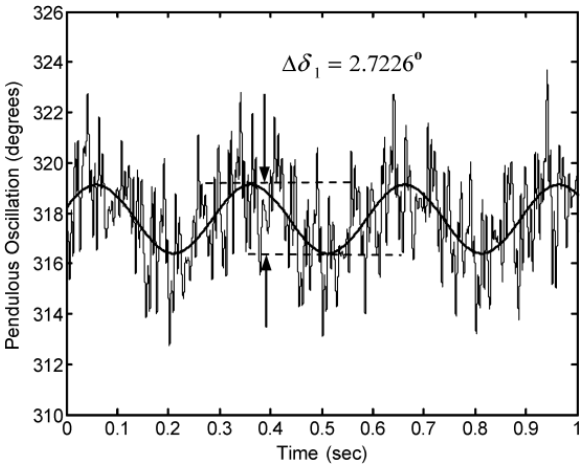

Fig 7. Pendulous oscillation and its fundamental component δ_1 (in degrees) versus time for the 5-hp motor for PWM excitation with two broken bars.

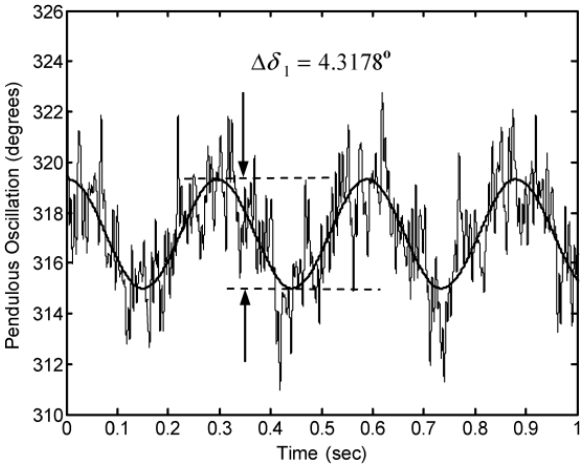

Fig 8. Pendulous oscillation and its fundamental component δ_1 (in degrees) versus time for the 5-hp motor for PWM excitation with three broken bars.

In Figs. 9 –11, the swing-angle index $\Delta\delta_1$ versus the number of broken bars are shown for the 5-hp motor under both PWM and sinusoidal excitations, as well as for the 2-hp motor under sinusoidal excitation, respectively. These figure demonstrate that there is always a difference between the resulting angle $\Delta\delta_1$ for a healthy cage and that angle of a cage with even one broken bar. Moreover, the severity of broken-bar faults can be evaluated using the swing-angle index. The latter characteristic of the swing-angle index makes it a more clear-cut tool for specific characterizing of bar breakage than the spectral-analysis approaches [25].

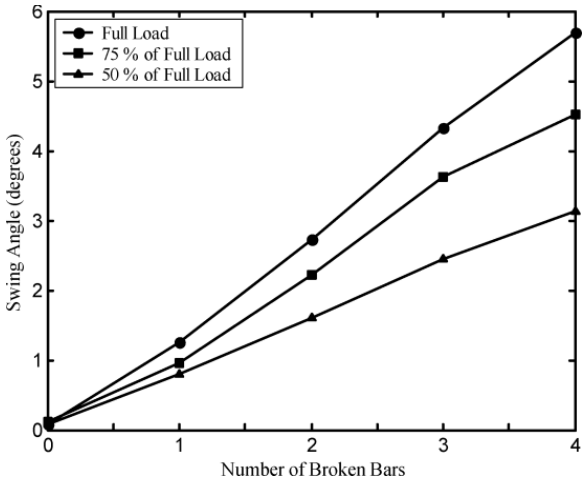

Fig 9. Swing angle $\Delta\delta_1$ versus number of broken bars for the PWM excitation of the 5-hp induction motor.

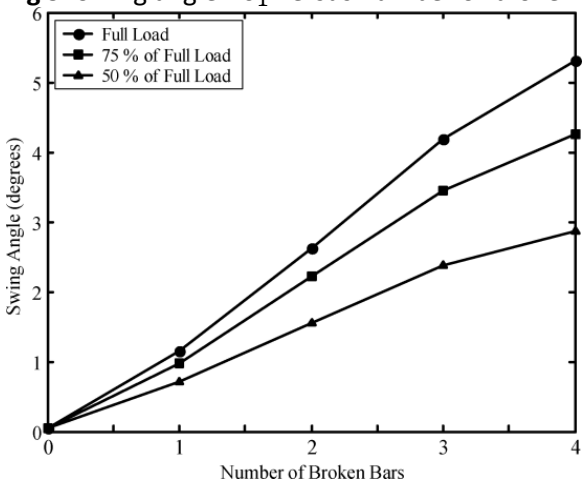

Fig 10. Swing angle $\Delta\delta_1$ versus number of broken bars for the sinusoidal excitation of the 5-hp induction motor.

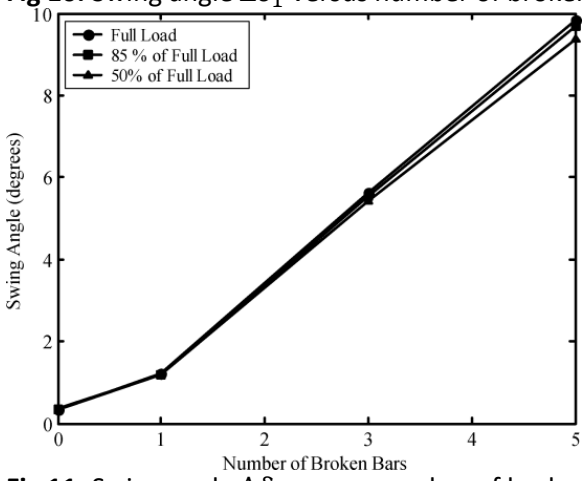

Fig 11. Swing angle $\Delta\delta_1$ versus number of broken bars for the sinusoidal excitation of the 2-hp induction motor.

B. Interturn Fault Diagnostics

As representative examples of the many tests performed on the 2- and 5-hp induction motors in the laboratory, the pendulous oscillations of the 2-hp induction motor in an enlargement (zoom) polar-coordinate plot is shown in Fig 12, for a five-turn (2.31% of winding) fault, while the short circuit was through a 0.8-Ω external resistor, $r_f = 0.8\Omega$. As one can see in Fig 12, an interturn fault generates an

unfilled-petal shape, while a filled-petal shape is generated in case of a broken-bar fault. This difference is due to the fact that the frequency of the pendulous oscillation due to interturn faults is twice the line frequency ($2f_1$), which matches the frequency of amplitude modulation of r, which is also equal to $2f_1$ [31]. Hence, the result is the unfilled-petal shape (see Fig 13). In other words, at any angle δ, the r quantity will not change from zero to its maximum value because r and δ are varying with time simultaneously [see Fig 13(b)]. Therefore, in this case, the polar plot of (r, δ) constitutes only the outer boundary of the petal shape. However, in case of a broken-bar fault, for any angle δ, the r value is changing from zero to its maximum value [see Fig 13(a)]. Therefore, in this case, the polar plot has a filled-petal shape.

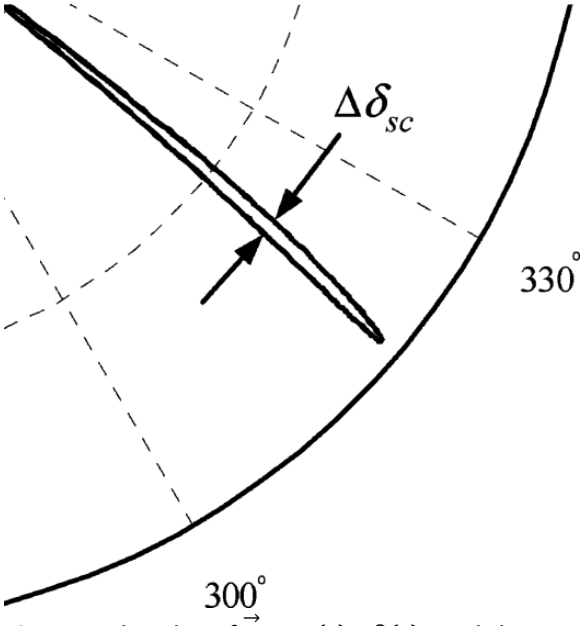

Fig 12. Polar plot of $\vec{r} = r(t)\angle\delta(t)$, and the swing angle $\Delta\delta_{\mathrm{sc}}$ (in degrees) in the case of five interturn faults of the 2-hp motor at full-load condition.

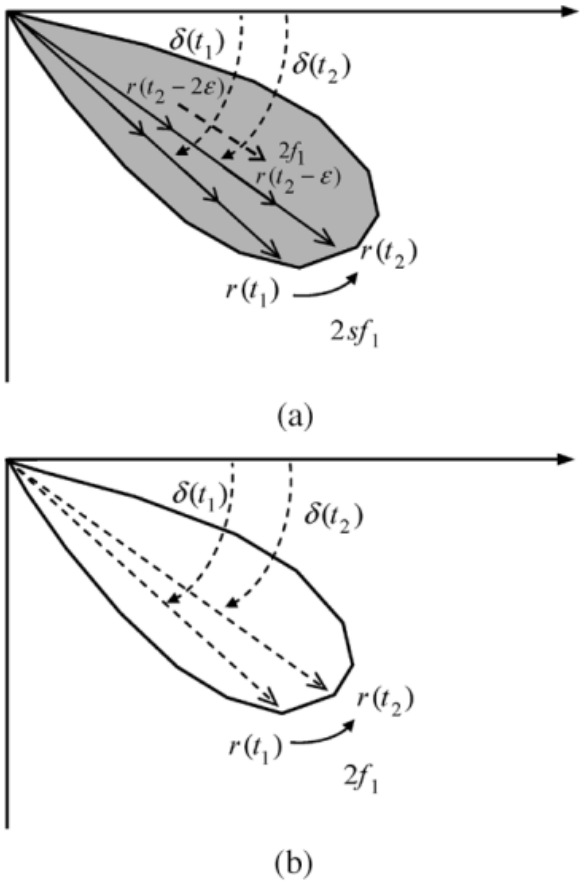

Fig 13. Polar plots of the (r, δ) vector in cases of (a) broken-bar and (b) interturn short-circuit faults.

Moreover, a degree of curvature can be observed in the petal shape of Fig 12, which is due to the existence of the external resistor. The external resistor was used in those tests to restrict the shorted loop current to an immune (safe) level of current that does not cause permanent coil damage. A similar type of curvature was observed by these authors in the polar plot (r, δ) of the pendulous oscillation in the presence of unbalances in the power-supply voltage amplitudes [31]. Accordingly, in the calculation procedure of the swing angle $\Delta\delta_{\mathrm{sc}}$, the maximum thickness of the petal shape is used as the interturn-fault diagnostic index to avoid any error in the fault diagnosis, which may be caused by the curvature effect. In this procedure, the radius, $r = \mathrm{abs}(\mathrm{Re}(\vec{i}_{\mathrm{s}}))$, is divided into several piecewise segments $[r_o, r_o + \Delta r, \dots, r_o + n\Delta r]$, and for each segment in the polar plot, the maximum value of the swing angle $\Delta\delta(r_k)$, $k = 0,1, \dots, n$, is calculated, while the swing-angle index $\Delta\delta_{\mathrm{sc}}$ is the maximum value of $\Delta\delta(r_k)$. Thus, for each power cycle, a single value for the swing angle $\Delta\delta_{\mathrm{sc}}$ is obtained. For comparison purposes, the negative sequence component I_{n} of the line current is also obtained for each power cycle. The results of the online interturn-fault detection for two case studies of 5- and 2-hp induction motors are shown in Figs. 14 –17, where $r_{\mathrm{f}} = 1\Omega$ in the case of the 5-hp motor and $r_{\mathrm{f}} = 0.8\Omega$ in the case of the 2-hp motor. As one can see in Figs. 14 and 16, an interturn fault can be easily detected using the swing-angle index only if the amplitude If of the circulating current exceeds the amplitude IL of the line current. Also, Fig 15 shows that the negative sequence component I_{n} of current is reliable enough for interturn-fault detection in the case study of the 5-hp motor. However, this index leads to an uncertainty in the case of the 2-hp motor (see Fig 17), which inherently

possessed a degree of construction imperfection due to its random winding nature. However, as can be seen in Figs. 14 and 16, the swing-angle index $\Delta\delta_{\mathrm{sc}}$ can indicate an interturn fault for both the 2- and 5-hp motors if the amplitude of the circulating current I_{f} exceeds the line current I_{L}. It should be noted that if the circulating short-circuit current I_{f} increases beyond the line current I_{L}, the shorted portion of the phase coil demagnetizes the rest of the impacted phase. Meanwhile, the peaks of the instantaneous line current and the circulating current if do not occur at the same instance. Accordingly, the demagnetizing effect of the circulating current does not disturb the peak current of the impacted phase in a significant manner. However, the swing angle $\Delta\delta_{\mathrm{sc}}$ is not based on only the peak values of the three-phase currents. In other words, the swing angle is obtained based on the maximum thickness of the polar plot (r, δ).

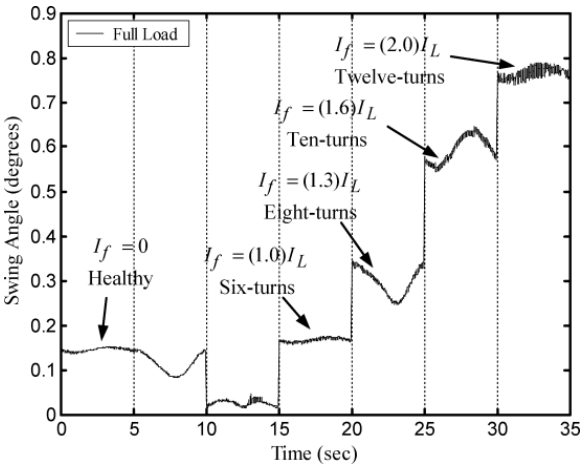

Fig 14. Swing angle $\Delta\delta_{\mathrm{sc}}$ (in degrees) versus time (in seconds) for the sinusoidal excitation of the 5-hp induction motor.

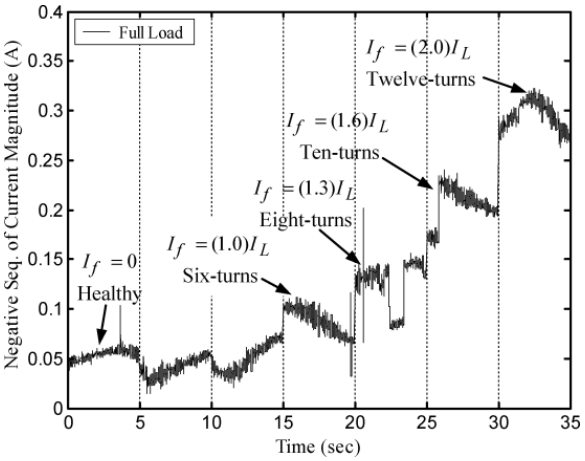

Fig 15. Negative-sequence component of current magnitude I_{n} (in amperes) versus time (in seconds) for the sinusoidal excitation of the 5-hp induction motor.

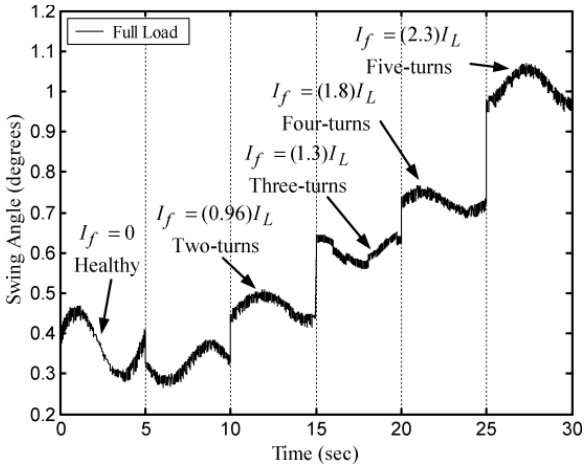

Fig 16. Swing angle $\Delta\delta_{\mathrm{sc}}$ (in degrees) versus time (in seconds) for the sinusoidal excitation of the 2-hp induction motor.

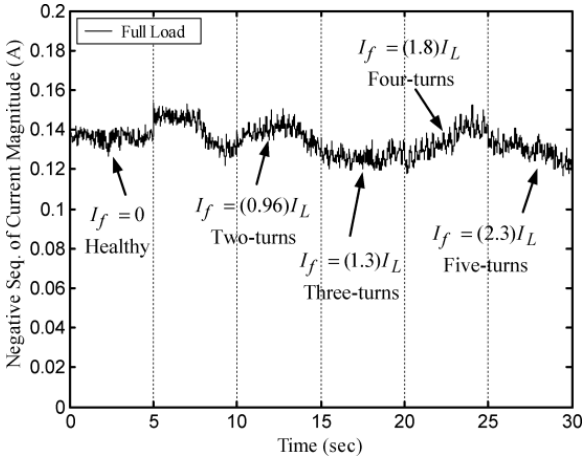

Fig 17. Negative-sequence component of current magnitude I_{n}In (in amperes) versus time (in seconds) for the sinusoidal excitation of the 2-hp induction motor.

In Tables II and III, the average values of the swing-angle index $\Delta\delta_{\mathrm{sc}}$ (in degrees), the peak value of the negative-sequence component I_n of the stator line currents (in amperes), the peak value of the negative sequence component of the terminal line-to-line voltages V_n (in volts), the peak value of the positive sequence component I_{p} of the stator line currents (in amperes), and the peak of the short-circuit loop current I_{f} are given in terms of the percentage of the STs ratio (ST%). It is clear that, using the swing-angle index, the interturn faults can be detected only when I_{f} exceeds I_{p} (or the line current I_{L}). Also, from TABLE II, It can be observed that the negative-sequence index In can indicate an interturn fault only if the STs exceed the threshold of 2.5% of the total number of turns per phase. From TABLE III, for the case of the 2-hp motor, it can be observed that the maximum number of STs did not exceed 2.31% of the total number of turns per phase, which is below the 2.5% threshold mentioned above, and the negative sequence index could not indicate any interturn fault in this case. However, the corresponding short-circuit circulating current I_{f} is more than twice the magnitude of the line current for the five-turn fault (i.e., 2.31%) in the 2-hp motor (see TABLE III). In other words, the negative sequence component index I_{n} is a direct function of the STs, and not a function of the circulating loop-current ratio $I_{\mathrm{f}}/I_{\mathrm{L}}$. However, the swing-angle index is a function of the circulating loop-current ratio $I_{\mathrm{f}}/I_{\mathrm{L}}$. This shows the strength of the concept of the swing-angle index $\Delta\delta_{\mathrm{sc}}$ presented and

chosen here for detecting incipient interturn faults. In order to present more evidences, the laboratory measurements were done for the different load levels, and the results are demonstrated in Figs. 18 – 21 for the case studies of the 5- and 2-hp induction motors, respectively. It should be pointed out that the current amplitude If indicates the severity of an interturn fault, not the STs ratio by itself. It has to be mentioned that the rewound 5-hp motor was built to a degree of perfection to render it a near perfectly balanced machine under healthy condition, while the 2-hp induction motor had a degree of construction imperfections. Again, it should be observed that Figs. 18 and 20 show the "clear-cut" nature of the swing-angle index for diagnosing interturn faults in both the 5- and 2-hp motors, despite the winding imperfections of the latter. This is not the case according to the test data depicted in Figs. 19 and 21 for the negative sequence current as a fault-identification index, particularly for the 2-hp motor with a slight unbalance in the three-phase windings.

TABLE II Characteristics of the 5-hp Motor Under Full-Load Conditions

ST (%)	$\Delta\delta_{sc}^{\circ}$	I_n (A)	V_n (V)	I_p (A)	I_f (A)
0.00	0.1449	0.0541	1.1237	9.2669	0.00
0.83	0.0252	0.0408	1.1765	9.2507	3.09
1.66	0.1252	0.0495	1.1765	9.2534	6.18
2.50	0.1668	0.0874	1.2863	9.2753	9.28
3.33	0.2973	0.1261	1.1204	9.2763	12.37
4.16	0.5960	0.2053	1.3123	9.1899	15.47
5.00	0.7652	0.2955	1.4401	9.2436	18.56

TABLE III Characteristics of the 2-hp Motor Under Full-Load Conditions

ST (%)	$\Delta\delta_{sc}^{\circ}$	I_n (A)	V_n (V)	I_p (A)	I_f (A)
0.00	0.3742	0.1363	3.2882	3.7162	0.00
0.46	0.3282	0.1403	1.9624	3.7960	1.73
0.93	0.4676	0.1382	1.3821	3.7040	3.57
1.39	0.6082	0.1265	2.8478	3.7289	5.21
1.85	0.7273	0.1342	3.0026	3.7278	6.94
2.31	1.0147	0.1295	2.1435	3.7163	8.68

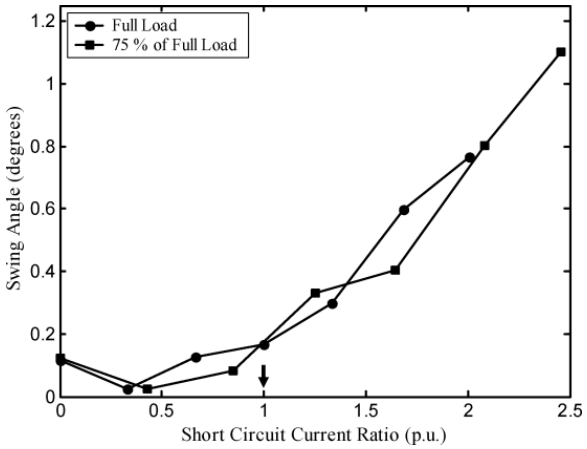

Fig 18. Swing angle $\Delta\delta_{\mathrm{sc}}$ (in degrees) versus the short-circuit ratio $I_{\mathrm{f}}/I_{\mathrm{L}}$ for the 5-hp induction motor.

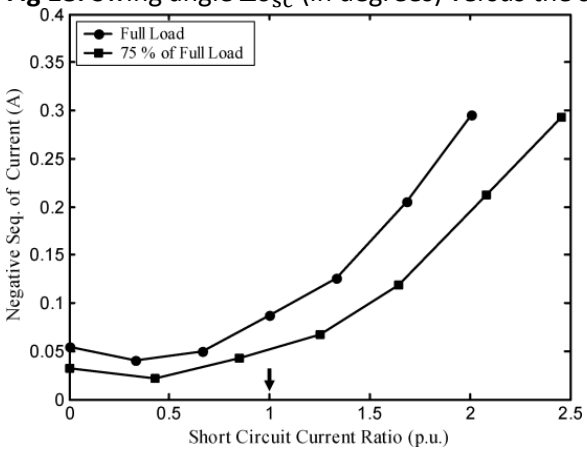

Fig 19. Negative-sequence component of current magnitude I_{n} (in amperes) versus the short-circuit current ratio $I_{\mathrm{f}}/I_{\mathrm{L}}$ for the 5-hp induction motor.

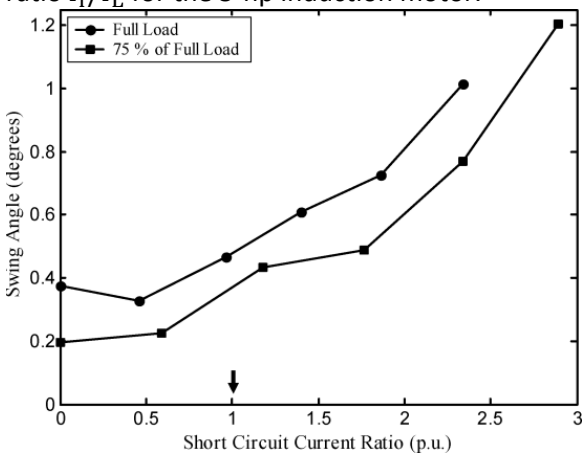

Fig 20. Swing angle $\Delta\delta_{\mathrm{sc}}$ (in degrees) versus the short-circuit ratio $I_{\mathrm{f}}/I_{\mathrm{L}}$ for the 2-hp induction motor.

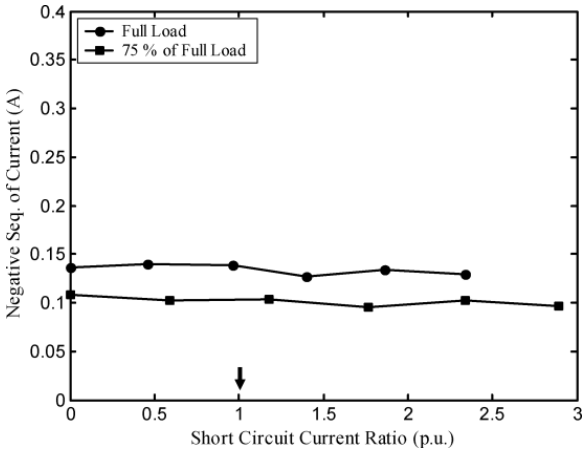

Fig 21. Negative-sequence component of current magnitude I_{n} (in amperes) versus the short circuit ratio $I_{\mathrm{f}}/I_{\mathrm{L}}$ for the 2-hp induction motor.

SECTION IV. Conclusion

Robust interturn and broken-bar fault diagnostic techniques based on the motor's magnetic-field space-vector pendulous-oscillation concept have been introduced and examined for two case studies of 2- and 5-hp induction motors. The experimental results have shown the strength and fidelity of

these techniques. It was also shown that the swing angle $\Delta\delta_{sc}$ is a function of the ratio between the short-circuit circulating current and the line (phase) current in case of stator partial STs. Moreover, an interturn fault can be detected if the circulating current increases slightly beyond the phase-current level, even before the occurrence of higher levels of damaging circulating currents. Meanwhile, the experimental results confirmed that through using the swing angle $\Delta\delta_1$, even the subtle fault of one broken bar can be distinguished (detected) from a healthy rotor cage. Hence, the swing-angle indexes $\Delta\delta_{sc}$ and $\Delta\delta_1$ have been demonstrated to be "clear-cut" means that enable one to detect stator interturn and rotor broken-bar faults at an early stage to prevent further damage to the machine and involved systems.

ACKNOWLEDGMENT

The authors wish to thank Dr. P. Schmidt and Dr. F. Discenzo of Rockwell Corporation in providing the 5-hp test motors and providing access to their laboratory facilities. The authors also wish to thank R. Bartos, S. Dellinger, and Dr. D. Ionel of A. O. Smith Corporation for providing the 2-hp test motor and providing access to their laboratory facilities.

Appendix

Characteristics of the 5- and 2-hp induction motors properties.

Design Feature	2-hp IM	5-hp IM
Power (hp)	2	5
Voltage (V)	230/460	230/460
Current (A)	5.4/2.7	13.6/6.8
Speed (r/min)	3450	1165
Number of Poles	2	6
Number of coils per phase	8	6
Number of Turns per Phase	216	240
Type of Stator Windings	Concentrated	Lap
Number of Rotor Bars	36	45
Number of Stator Slots	24	36

References

1. W. Deleroi, "Squirrel cage motor with broken bar in the rotor-Physical phenomena and their experimental assessment", Proc. Int. Conf. Electrical Machines, pp. 700-767, 1982-Sep.
2. W. Deleroi, "Der stabbruch im kaufiglaufer eines asychonomotor", *Arch. Elektrotech.*, vol. 67, pp. 91-99, 1984.
3. S. Williamson and A. C. Smith, "Steady state analysis of 3-phase cage motors with rotor broken bar and end ring faults", *Proc. Inst. Elect. Eng.*, vol. 129, no. 3, pp. 93-100, May 1982.
4. S. Williamson and K. Mirzoian, "Analysis of cage induction motors with stator winding faults", *IEEE/PES Summer Meeting*, 1984-Jul.-15.
5. S. Williamson and K. Mirzoian, "Analysis of cage induction motors with stator winding faults", *IEEE Trans. Power App. Syst.*, vol. PAS-104, no. 7, pp. 1838-1842, Jul. 1985.

6. G. B. Kliman, R. A. Koegl, J. Stein, R. D. Endicott and M. W. Madden, "Noninvasive detection of broken rotor bars in operating induction machines", *IEEE Trans. Energy Convers.*, vol. 3, no. 4, pp. 873-879, Dec. 1988.
7. G. B. Kliman, W. J. Premerlani, R. A. Koegl and D. Hoeweler, "A new approach to on-line fault detection in AC motors", *Proc. IEEE-IAS Annu. Meeting*, pp. 687-693, 1996-Oct.-6.
8. A. Bellini, F. Fillippetti, G. Franceschini, C. Tassoni and G. B. Kliman, "Quantitative evaluation of induction motor broken bars by means of electrical signature analysis", *IEEE Trans. Ind. Appl.*, vol. 37, no. 5, pp. 1248-1255, Sep./Oct. 2001.
9. F. C. Trutt, J. Sottile and J. L. Kohler, "Online condition monitoring of induction motors", *IEEE Trans. Ind. Appl.*, vol. 38, no. 6, pp. 1627-1632, Nov./Dec. 2002.
10. C. Kral, F. Pirker and G. Pascoli, "Detection of rotor faults in squirrel-cage induction machines at standstill for batch tests by means of the Vienna monitoring method", *IEEE Trans. Ind. Appl.*, vol. 38, no. 3, pp. 618-624, May/Jun. 2002.
11. R. R. Schoen, B. K. Lin, T. G. Habetler, J. H. Schlag and S. Farag, "An unsupervised on-line system for induction motor fault detection using stator current monitoring", *IEEE Trans. Ind. Appl.*, vol. 31, no. 6, pp. 1280-1286, Nov./Dec. 1995.
12. S. B. Lee, R. M. Tallam and T. G. Habetler, "A robust on-line turn-fault detection technique for induction machines based on monitoring the sequence impedance matrix", *IEEE Trans. Power Electron.*, vol. 18, no. 3, pp. 865-872, May 2003.
13. P. Vas, "Parameter estimation" in Condition Monitoring and Diagnosis of Electrical Machines, New York:Oxford Univ. Press, 1993.
14. M. E. H. Benbouzid and G. B. Kliman, "What stator current processing-based technique to use for induction motor rotor faults diagnosis?", *IEEE Trans. Energy Convers.*, vol. 18, no. 2, pp. 238-244, Jun. 2003.
15. D. Kostic-Perovic, M. Arkan and P. Unsworth, "Induction motor fault detection by space vector angular fluctuation", *Conf. Rec. IEEE-IAS Annu. Meeting*, vol. 1, pp. 388-394, 2000.
16. M. Arkan, D. K. Perovic and P. Unsworth, "Online stator fault diagnosis in induction motors", *Proc. Inst. Elect. Eng.-Electr. Power Appl.*, vol. 148, no. 6, pp. 537-547, Nov. 2001.
17. C. Demian, A. Mpanda-Mabwe, H. Henao and G.-A. Capolino, "Detection of induction machines rotor faults at standstill using signals injection", *IEEE Trans. Ind. Appl.*, vol. 40, no. 6, pp. 1550-1559, Nov./Dec. 2004.
18. H. Henao, C. Martis and G. A. Capolino, "An equivalent internal circuit model of the induction machine for advanced spectral analysis", *IEEE Trans. Ind. Appl.*, vol. 40, no. 3, pp. 726-734, May/Jun. 2004.
19. S. M. A. Cruz and A. J. M. Cardoso, "Stator winding fault diagnosis in three-phase synchronous and asynchronous motors by the extended Park's vector approach", *IEEE Trans. Ind. Appl.*, vol. 37, no. 5, pp. 1227-1233, Sep./Oct. 2001.
20. S. Nandi and H. A. Toliyat, "Novel frequency-domain-based technique to detect stator interturn faults in induction machines using stator-induced voltages after switch-off", *IEEE Trans. Ind. Appl.*, vol. 38, no. 1, pp. 101-109, Jan./Feb. 2002.
21. A. Stavrou, H. G. Sedding and J. Penman, "Current monitoring for detecting inter-turn short circuits in induction motors", *IEEE Trans. Energy Convers.*, vol. 16, no. 1, pp. 32-37, Mar. 2001.

22. W. T. Thomson, D. Rankin and D. G. Dorrell, "On-line current monitoring to diagnose airgap eccentricity in large three-phase induction motors-industrial case histories verify the predictions", *IEEE Trans. Energy Convers.*, vol. 14, no. 4, pp. 1372-1378, Dec. 1999.
23. B. K. Gupta and I. M. Culbert, "Assessment of insulation condition in rotating machine stators", *IEEE Trans. Energy Convers.*, vol. 7, no. 3, pp. 500-508, Sep. 1992.
24. B. Mirafzal and N. A. O. Demerdash, "Induction machine broken-bar fault diagnosis using the rotor magnetic field space vector orientation", *IEEE Trans. Ind. Appl.*, vol. 40, no. 2, pp. 534-542, Mar./Apr. 2004.
25. B. Mirafzal and N. A. O. Demerdash, "Effects of load Magnitude on diagnosing broken bar faults in induction motors using the pendulous oscillation of the rotor magnetic field orientation", *IEEE Trans. Ind. Appl.*, vol. 41, no. 3, pp. 771-783, May/Jun. 2005.
26. H. A. Toliyat and T. A. Lipo, "Transient analysis of cage induction machines under stator rotor bar and end ring faults", *IEEE Trans. Energy Convers.*, vol. 10, no. 2, pp. 241-247, Jun. 1995.
27. J. F. Bangura and N. A. O. Demerdash, "Diagnosis and characterization of effects of broken bars and connectors in squirrel-cage induction motors by a time-stepping coupled finite element-state space modeling approach", *IEEE Trans. Energy Convers.*, vol. 14, no. 4, pp. 1167-1176, Dec. 1999.
28. "Report of large motor reliability survey of industrial and commercial installation Part I", *IEEE Trans. Ind. Appl.*, vol. IA-21, no. 4, pp. 853-864, Jul./Aug. 1985.
29. "Report of large motor reliability survey of industrial and commercial installation Part II", *IEEE Trans. Ind. Appl.*, vol. IA-21, no. 4, pp. 865-872, Jul./Aug. 1985.
30. P. F. Albrecht, J. C. Appiarius and D. K. Sharma, "Assessment of the reliability of motors in utility applications-Updated", *IEEE Trans. Energy Convers.*, vol. EC-1, no. 1, pp. 39-46, Dec. 1986.
31. B. Mirafzal, "Incipient fault diagnosis in squirrel-cage induction motors", Aug. 2005.